euspen's 22nd International Conference & Exhibition, Geneva, CH, May/June 2022
www.euspen.eu

New insights into the mechanisms of ultrasonic vibration cutting of brittle materials via multi-cyclic nanoindentation

Weihai Huang and Jiwang Yan*

Department of Mechanical Engineering, Faculty of Science and Technology, Keio University, Yokohama 223-8522, Japan

** yan@mech.keio.ac.jp*

Abstract
Ultrasonic vibration cutting is a potential method for ductile machining of brittle materials. Although there are some research works trying to answer why the ultrasonic vibration promotes ductile machining of brittle materials, most of them are based on geometrical and kinematic analysis. In this study, plunge-cutting experiments under the conventional and vibration-assisted cutting conditions were conducted on single crystalline silicon and the results were compared to those of multi-cyclic nanoindentation tests. The surface morphology and subsurface microstructure of both machined grooves and residual indents were characterized. Results of plunge-cutting experiments show that with ultrasonic vibration cutting, the critical depth of cut for ductile-to-brittle transition and the amorphous phase in cutting chips are increased compared with conventional cutting. Results of multi-cyclic nanoindentation tests show that the indentation-induced amorphous layer increased as the cyclic number increased, which is consistent with the cutting results. The findings from this study may help understand the removal mechanism of brittle materials during ultrasonic vibration cutting.

Ultrasonic vibration cutting, Cutting mechanisms, Ductile machining, Brittle materials, Cyclic nanoindentation

1. Introduction

Ultrasonic vibration-assisted diamond turning (UVDT) has been regarded as a promising technology for efficiently machining ferrous materials such as hardened steel and high-entropy alloy, as well as hard-brittle materials such as tungsten carbide, optical glass, and silicon carbide [1,2]. It has been demonstrated that UVDT can suppress the tool wear in machining of ferrous metals and improve the critical depth of cut in machining hard-brittle materials [3,4]. Recently, the development of various UVDT systems have been reported by many researchers [5-7].

In parallel, the machining mechanisms of UVDT process is also a hot research topic for decades. Shamoto et al. [8] supposed that the intermittent cutting due to the ultrasonic vibration causes the separation of the tool rake face from the chip. Owing to the tool-chip separation induced aerodynamic lubrication between the tool rake face and the chip, the friction at the tool-chip interface is reduced; meanwhile the instantaneous cutting force, which may cause materials brittle fracture, is reduced as well. Nath et al. [9] developed a predictive model for the maximum thickness of cut (TOC_m) of the workpiece material in the ultrasonic elliptical vibration cutting process, taking into consideration of the cutting speed, the tool vibration frequency, and the vibration amplitudes. They found that to achieve the ductile finishing of brittle materials, the TOC_m must be smaller than the critical depth of cut. Huang et al. [10] proposed a concept of ductile-regime machining in the ultrasonic elliptical vibration cutting of brittle materials. They believe that owing to the elliptical vibration locus, there is a space between the locus and the plane of machined surface, which can tolerate the crack propagation. Those cracks in the tolerable space will be removed by the next locus of cut, as long as the cracks do not penetrate into the plane of the machined surface. Therefore, ultrasonic elliptical vibration cutting could improve the critical depth of cut of brittle materials. Wang et al. [11] reported an optimal nominal cutting speed and vibration amplitudes which show significant impacts on the ductile-to-brittle transition behaviour in the ductile-regime elliptical vibration cutting of brittle materials. However, the above mentioned machining mechanisms are investigated from the aspect of geometry and kinematics. The material deformation behaviour of UVDT process have not been considered. Arefin et al. [12] investigated the chip formation, the forces, and the corresponding machined surfaces of 1D vibration cutting by Finite Element (FE) simulation. Liu et al. [13] established an effective tool rake angle model and applied molecular dynamics (MD) simulation to reveal the material removal mechanism in elliptical vibration cutting of brittle materials. However, up to date no experimental studies are available which focus on the material deformation behaviour in UVDT process.

The challenge of experimental study on the machining mechanism of UVDT process is that the evolution of material deformation caused by the cumulative intermittent cutting is difficult to be in-situ characterized. As an alternative to the intermittent cutting, multi-cyclic nanoindentation is effective to clarify the machining mechanisms of cyclic loading/unloading. Although there is some literature about the multi-cyclic nanoindentation of brittle materials, such as zirconia [14], germanium [15], and silicon [16], the relationship between the multi-cyclic nanoindentation results and the vibration cutting results have not been associated with each other.

In this study, plunge-cutting experiments under the conventional and vibration-assisted cutting conditions and the multi-cyclic nanoindentation tests are conducted on a typical brittle material, single-crystalline silicon. The surface morphology and subsurface microstructure of both the

machined grooves and the residual indents are characterized. The material deformation behaviour in vibration cutting process is explored by combining analysis of plunge-cutting experiments results with multi-cyclic nanoindentation tests results.

2. Material and methods

2.1. Material

A *p*-type boron-doped single-crystal silicon (100) wafer was used as the workpiece. The workpiece surface was polished to a smooth finish with a surface roughness of <2 nm Sa in a field of 360 × 360 μm^2.

2.2. Plunge-cutting experiment

Plunge-cutting experiments were conducted using an ultraprecision lathe (ASP-15, NACHI-FUJIKOSHI Co., Ltd., Japan) [17]. As illustrated in Figure 1(a), a silicon wafer was fixed on an aluminum block with a slight inclination, the inner side of which 14 mm away from the center of spindle. The depth of cut is therefore increased gradually as the spindle rotates. The feed rate in the x direction is chosen to be large enough so that the grooves are cut without interference. The spindle rotation rate was set to 20 rpm. A diamond tool with a nose radius of 0.9 mm was mounted to an ultrasonic tooling system (UTS2, Son-X Company, Germany) which can produce the vibration of tool at a frequency of 101.68 kHz with the resonance amplitude of 1.0 μm [1]. When the ultrasonic tooling system was turned off, the microgrooves were machined under conventional cutting condition.

After the plunge-cutting tests, the possible phase changes of the machined grooves were characterized using a laser micro Raman spectroscope, (inVia Raman, Renishaw Plc., UK). The 3D topography of the grooves was measured using a white light interferometer (Talysurf CCI 1000, Taylor Hobson Ltd., UK).

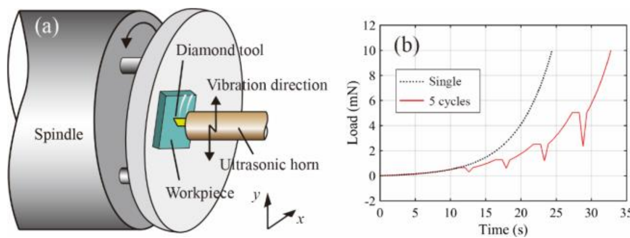

Figure 1. (a) Schematic model of a microgroove plunge-cut with a round-nosed tool. (b) The load-time curves of single nanoindentation and 5 cycles multi-cyclic nanoindentation.

2.3. Multi-cyclic nanoindentation test

Multi-cyclic nano-indentation tests were performed using a nanoindentation instrument (iNano, KLA Corporation, USA) equipped with a Berkovich diamond tip. The tip radius was estimated to be ~40 nm [18]. For the single indentation cycle, a maximum indentation load (P_{max}) of 10 mN was used. For multi indentation cycles, the P_{max} of each cycle is listed in Table 1. The holding time at the maximum indentation load for each cycle was 1 second. Figure 1(b) presents the load-time curves of single and 5 cycles multi-cyclic nanoindentation. The load curve follows the rule of constant indentation strain rate through continuous stiffness measurement (CSM) method. The load (P) equation is expressed in the following form,

$$\frac{\frac{\partial P}{\partial t}}{P} = \text{constant} \tag{1}$$

After the nanoindentation tests, the residual indents were characterized using an atomic force microscope (AFM), (AFM5100 N, Hitachi High-Technologies Corp., Japan). The possible phase changes of the residual indents were characterized using the inVia Raman spectroscope.

Table 1 Maximum load (P_{max}) of each indentation cycle in multi-cyclic nanoindentation.

	Total number of cycles	1st cycle	2nd cycle	N th cycle	Last cycle
P_{max} (mN)	2 cycles	5	10	-	10
	5 cycles	$10/2^4$	$10/2^3$	$10/2^{5-N}$	10
	10 cycles	$10/2^9$	$10/2^8$	$10/2^{10-N}$	10
	20 cycles	$10/2^{19}$	$10/2^{18}$	$10/2^{20-N}$	10

3. Results

3.1. Topography of microgrooves

Figure 2(a) and (b) show three-dimensional topographies of microgrooves on the silicon wafer plunge-cut under conventional and vibration cutting conditions. From the left to the right of the figure, as the depth of cut increases, the microgroove is gradually broadened. It can be also seen that the groove machined under the vibration cutting condition has a smoother edge as compared to that under the conventional cutting condition, although both grooves were cut by the same tool edge at the same conditions except the ultrasonic vibration. This phenomenon is similar to that reported in the UVDT of glass [8], which indicates that the material removal becomes more ductile at the vibration-assisted cutting condition.

Then, the critical depth of cut where the ductile-brittle transition occurred were measured from the cross-sectional profiles of the microgrooves. The critical depths of cut were 43 nm and 135 nm under conventional and vibration cutting conditions, which indicates that vibration cutting increases the critical depth cut by 3 times.

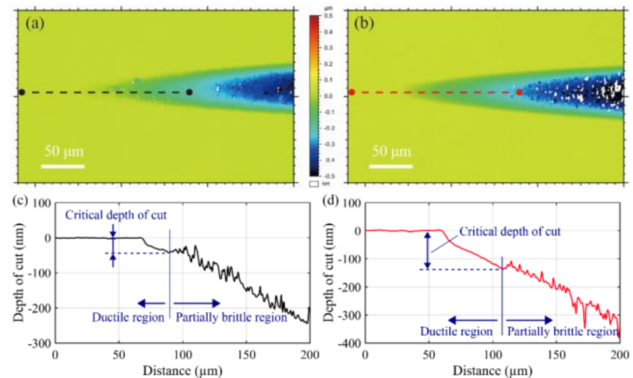

Figure 2. Three-dimensional topographies of the microgroove plunge-cut at (a) conventional cutting condition, and (b) vibration cutting condition. (c) and (d) are the profiles of the microgroove grooves corresponding to (a) and (b). (The white spots in (c) and (d) indicate lack of data, which is caused by the surface damages.)

3.2. Raman spectroscopy of microgrooves

Figure 3(a) shows the Raman spectra of the microgrooves plunge-cut under conventional and vibration cutting conditions. The laser micro-Raman tested points are within the ductile region of the microgrooves. It can be seen that each spectrum only exhibits strong peak around 520 cm^{-1}, corresponding to the single crystalline silicon (*c*-Si). However, the intensity of the crystalline silicon under the vibration cutting condition is slightly weaker than that under the conventional cutting condition. Meanwhile, its intensity at the shift of about 475 cm^{-1} which corresponds to the amorphous silicon(*a*-Si) is slightly stronger. These results indicate that vibration cutting will cause higher extent of amorphization beneath the machined surface.

Besides, the cutting chips adhered on the machined surface are measured by the Raman microscope as well, as presented in Figure 3(b). It can be seen that there exist two main peaks corresponding to *a*-Si and *c*-Si under both cutting conditions. This fact agrees with previous results where partly amorphous and partly crystalline chips are generated in ductile cutting of silicon [19]. Since the absolute Raman intensities varied with the density and size of the chip cluster, the Raman analysis of cutting chip is based on the peak intensity ratio (*r*). The Raman peak intensity ratio *r* is defined by:

$$r = I_a/I_c \qquad (2)$$

where I_a is the intensity of the amorphous silicon peak, and I_c is the intensity of the crystalline silicon peak.

Results show that the Raman peak intensity ratio under conventional cutting and vibration cutting conditions are 1.097 and 1.179. The larger *r* under vibration cutting condition indicates that the intermittent cutting would promote the amorphization of silicon. This might be because, on the one hand, after the chip has been separated from the tool (unloading), a phase transformation from metallic state β-Sn (Si-II) to amorphous will take place in the chip material near the tool [19]. On the other hand, the intermittent cutting increases the number of separations between the material and tool.

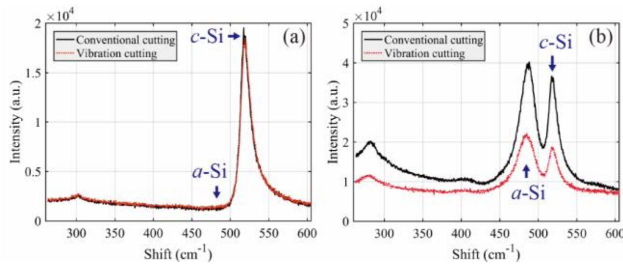

Figure 3. Raman spectrum of (a) ductile region of microgrooves, and (b) cutting chips.

3.3. Topography of residual indents

Figure 4(a1) – (e1) present typical load-depth curves obtained under single, 2 cycles, 5 cycles, 10 cycles, and 20 cycles nanoindentation tests, respectively. The occurrence of an elbow event, that is the slope of the unloading curve suddenly changes, was observed in all nanoindentation tests, which indicates that the Si-II phase formed during the loading process transforms into a-Si phase [20]. However, the pop-out event was not observed in all nanoindentation tests, which is different from the results reported by Fujisawa et al. [21]. In their study, during the cyclic nanoindentation of silicon with a maximum load of 10 mN, the pop-out event could occur when the applied force was unloaded to about 4 mN. The difference may be due to the different loading methods of the two studies.

Besides, it can be seen from insets of Figure 4(b1) and (c1) that in the previous cycle, the indentation depth decreased when the applied force unloaded to the minimum value; and then in the current cycle, when the applied force started to reload to the value the same as previous cycle, the indentation depth gradually increased and reached the same depth as before the previous cycle unloaded as well. This indicates that the material deformed only within the elastic range during the initial stage of each cycle of subsequent loading.

Figure 4(a2) – (e2) and their insets show the cross-sectional profiles of residual indents and the corresponding AFM morphologies of the residual indents. The locations of the cross-sectional profiles were indicated as black lines in the insets. It can be seen from the each inset that three pileups formed next to the three planes of residual indents, but the size and height of the three pileups are different due to the anisotropy of silicon. The cross-sectional profiles assist in quantitatively analyzing the height of pile-ups and the depth of residual indents. Results show that in all cases the height of pile-ups are about 15 nm, and the depth of residual indents are about 35 nm, which indicates that both the height of pile-ups and the depth of residual indents are independent of number of cycles of indentation.

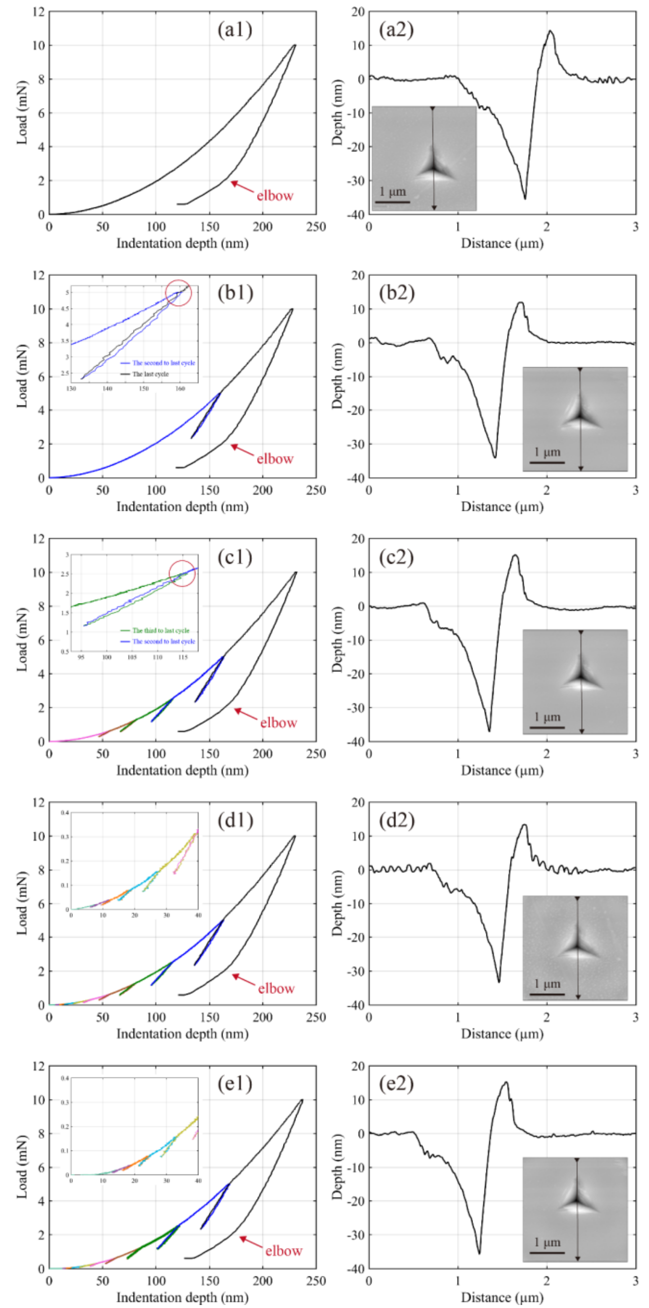

Figure 4. Load-displacement curve of: (a1) single, (b1) 2 cycles, (c1) 5 cycles, (d1) 10 cycles, (e1) 20 cycles nanoindentation. (a2) – (e2) are the AFM line profiles obtained along black lines in their corresponding insets.

3.4. Raman spectroscopy of residual indents

Figure 5 shows the Raman spectra of the residual indents. It can be seen that all indentations caused the formation of *a*-Si phase, as evidenced by the existence of Raman peaks around 475 cm^{-1}. These results also support the viewpoint that elbow event is the signal of amorphous silicon formation. In general, as the cyclic number increased, the intensity of *a*-Si peak gradually increased, while the intensity of *c*-Si peak gradually decreased. However, as the number of indentation cycles increases further,

in particular from 5 to 20 cycles, the degree of amorphization almost no longer increases, and the crystallinity of *c*-Si no longer decreases as well.

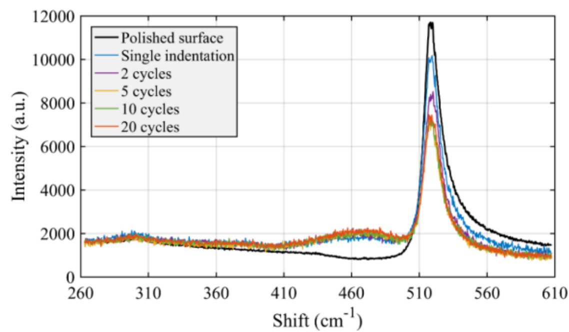

Figure 5. Raman spectra obtained from the polished surface and the residual indents corresponding to single nanoindentation and cyclic nanoindentations.

4. Discussion

The results of plunge-cutting experiment indicate that the intermittent cutting promotes the amorphization of chips, which has been explained from the viewpoint that the vibration cutting process increases the number of tool-workpiece impacts and separations, additionally the amorphous phase takes place during the tool-workpiece separations. Furthermore, the results of multi-cyclic nanoindentation test, i.e., the elbow occurred during unloading and the intensity of a-Si peak increased with the cyclic number, are consistent with the cutting results. However, according to the fact that the amorphization stops increasing as the number of cycles further increases in the nanoindentation tests, it can be supposed that there is an upper critical vibration frequency in the vibration cutting process, above which the degree of amorphous phase in chips will not increase anymore.

Besides, according to the load-displacement curves of indentations, it can be inferred that during the vibration cutting process there is a stage of complete elastic deformation when the tool separates from the workpiece material and contacts with workpiece material again. The cross-sectional profiles of indentations infer that in the case of the same cutting distance the vibration frequency of tool in vibration cutting process may not affect the volume of material deformation or removal.

5. Conclusions

Plunge-cutting tests and multi-cyclic nanoindentation tests have been made on single crystalline silicon. The surface morphology and subsurface microstructure of both machined grooves and residual indents were characterized and compared. The main conclusions are as follows:

(1) Compared with conventional cutting, the critical depth of cut for the ductile-to-brittle transition of silicon is increased by 3 times with ultrasonic vibration cutting.
(2) Ultrasonic vibration cutting caused more amorphous material in machined surface and cutting chips than the conventional cutting.
(3) As the cyclic number increased, the indentation-induced amorphous layer increased, but the growth rate decreased.
(4) Both the height of pile-ups and the depth of residual indents are independent of number of cycles of indentation.

This study attempts to characterize the deformation behaviour of silicon under multiple cyclic loading/unloading and correlates it with the ultrasonic vibration cutting process. The finding provides useful information for fundamental investigation of the mechanisms of material removal and chip formation in vibration cutting of brittle materials.

References

[1] Zhang, L., Hashimoto, T., Yan, J., 2021, Machinability exploration for high-entropy alloy FeCrCoMnNi by ultrasonic vibration-assisted diamond turning, *CIRP Annals*, **70**, 37-40.
[2] Zhang, J., Cui, T., Ge, C., Sui, Y., Yang, H., 2016, Review of micro/nano machining by utilizing elliptical vibration cutting, *International Journal of Machine Tools and Manufacture*, **106**, 109-126.
[3] Guo, J., Zhang, J., Pan, Y., Kang, R., Namba, Y., Shore, P., Yue, X., Wang, B., Guo, D., 2020, A critical review on the chemical wear and wear suppression of diamond tools in diamond cutting of ferrous metals, *International Journal of Extreme Manufacturing*, **2**, 012001.
[4] Zhang, J., Zhang, J., Liu, C., Chen, X., Xiao, J., Xu, J., 2020, Machinability of single crystal calcium fluoride by applying elliptical vibration diamond cutting, *Precision Engineering*, **66**, 306-314.
[5] Shamoto, E., Suzuki, N., Moriwaki, T., Naoi, Y., 2002, Development of Ultrasonic Elliptical Vibration Controller for Elliptical Vibration Cutting, *CIRP Annals*, **51**, 327-330.
[6] Guo, P., Ehmann, K.F., 2013, Development of a tertiary motion generator for elliptical vibration texturing, *Precision Engineering*, **37**, 364-371.
[7] Huang, W., Yu, D., Zhang, M., Ye, F., Yao, J., 2017, Analytical design method of a device for ultrasonic elliptical vibration cutting, *The Journal of the Acoustical Society of America*, **141**, 1238-1245.
[8] Moriwaki, T., Shamoto, E., Inoue, K., 1992, Ultraprecision Ductile Cutting of Glass by Applying Ultrasonic Vibration, *CIRP Annals*, **41**, 141-144.
[9] Nath, C., Rahman, M., Neo, K.S., 2011, Modeling of the Effect of Machining Parameters on Maximum Thickness of Cut in Ultrasonic Elliptical Vibration Cutting, *Journal of Manufacturing Science and Engineering*, **133**, 011007.
[10] Huang, W., Yu, D., Zhang, X., Zhang, M., Chen, D., 2018, Ductile-regime machining model for ultrasonic elliptical vibration cutting of brittle materials, *Journal of Manufacturing Processes*, **36**, 68-76.
[11] Wang, J., Yang, Y., Zhu, Z., Wang, Y., Liao, W., Guo, P., 2020, On ductile-regime elliptical vibration cutting of silicon with identifying the lower bound of practicable nominal cutting velocity, *Journal of Materials Processing Technology*, **283**, 116720.
[12] Arefin, S., Zhang, X., Kumar, A.S., Neo, D.W.K., Wang, Y., 2021, Study of chip formation mechanism in one-dimensional vibration-assisted machining, *Journal of Materials Processing Technology*, **291**, 117022.
[13] Liu, C., Zhang, J., Zhang, J., Chu, J., Chen, X., Xiao, J., Xu, J., 2021, Numerical investigation on material removal mechanism in elliptical vibration cutting of single-crystal silicon, *Materials Science in Semiconductor Processing*, **134**, 106019.
[14] Kosai, K., Yan, J., 2020, Effects of cyclic loading on subsurface microstructural changes of zirconia polycrystals in nanoscale mechanical processing, *International Journal of Machine Tools and Manufacture*, **159**, 103626.
[15] Kosai, K., Yan, J., 2019, Direct observations of multi-cyclic nanoindentation-induced phase transformations in single-crystal Ge, *Materials Research Express*, **6**, 075065.
[16] Huang, H., Yan, J., 2015, New insights into phase transformations in single crystal silicon by controlled cyclic nanoindentation, *Scripta Materialia*, **102**, 35-38.
[17] Huang, W., Yan, J., 2020, Surface formation mechanism in ultraprecision diamond turning of coarse-grained polycrystalline ZnSe, *International Journal of Machine Tools and Manufacture*, **153**, 103554.
[18] Huang, W., Yan, J., 2021, Deformation behaviour of soft-brittle polycrystalline materials determined by nanoscratching with a sharp indenter, *Precision Engineering*, **72**, 717-729.
[19] Yan, J., Asami, T., Harada, H., Kuriyagawa, T., 2009, Fundamental investigation of subsurface damage in single crystalline silicon caused by diamond machining, *Precision Engineering*, **33**, 378-386.
[20] Huang, H., Yan, J., 2015, On the mechanism of secondary pop-out in cyclic nanoindentation of single-crystal silicon, *Journal of Materials Research*, **30**, 1861-1868.
[21] Fujisawa, N., Williams, J.S., Swain, M.V., 2007, On the cyclic indentation behavior of crystalline silicon with a sharp tip, *Journal of Materials Research*, **22**, 2992-2997.